Landslides
DOI 10.1007/s10346-020-01376-9
Received: 17 October 2019
Accepted: 16 February 2020

S. A. Wall · J. J. Roering · F. K. Rengers

Runoff-initiated post-fire debris flow Western Cascades, Oregon

Abstract Wildfires dramatically alter the hydraulics and root reinforcement of soil on forested hillslopes, which can promote the generation of debris flows. In the Pacific Northwest, post-fire shallow landsliding has been well documented and studied, but the potential role of runoff-initiated debris flows is not well understood and only one previous to 2018 had been documented in the region. On 20 June 2018, approximately 1 year after the Milli fire burned 24,000 acres, a runoff-initiated debris flow occurred on the flanks of Black Crater in the Oregon Cascade Range. The debris flow was initiated via dispersed rilling on > 30-degree slopes near the crater rim and traveled > 1.5 km downslope. We measured exceptionally low soil infiltration rates at the study site, likely due to high burn severity during the Milli fire. Based on nearby 5-min rain gage data, we quantified rainfall rates for the storm event that triggered the debris flow. Our results show that peak 15-min rainfall rates were 25.4 mmh^{-1}, equaling or exceeding the measured infiltration rates at the study site, which had a geometric mean of ~ 24 mmh^{-1}. Field mapping shows that high burn severity resulted in the initiation of the debris flow and that convergent and steep topography promoted the development of a debris flow at this site. As wildfires increase in frequency and intensity across the western USA, the Pacific Northwest could become more susceptible to runoff-initiated debris flows. Therefore, characterization of the conditions that resulted in this debris flow is crucial for understanding how runoff-initiated debris flows may shape terrain and impact hazards in the Pacific Northwest.

Keywords Post-fire debris flow · Post-fire runoff · Wildfire · Oregon Cascades · Soil infiltration · Climate change

Introduction

As wildfires increase in frequency and intensity across the western USA, it is necessary to understand their fundamental impacts on hydrologic response, erosional processes, and hazards. Post-fire debris flows are one of the most destructive and potentially deadly consequences from wildfire's alteration of mountainous landscapes. There are two primary processes responsible for the initiation of post-fire debris flows: debris flows resulting from soil saturation and shallow landsliding (Swanson 1981; Wondzell and King 2003; Woodsmith et al. 2007; Jackson and Roering 2009) and runoff-initiated debris flows that mobilize from rainfall rates that exceed infiltration rates (Cannon and Gartner 2005; Parise and Cannon 2012). Runoff-initiated debris flows are a common response to high-intensity rainfall on burned hillslopes in Mediterranean climates (Inbar et al. 1998; Wondzell and King 2003; Kampf et al. 2016). In the USA, such debris flows have been widely documented in southern California, the Rocky Mountains, and Interior Northwest, which includes parts of eastern Oregon and Idaho (Wondzell and King 2003; Cannon and Gartner 2005; Jordan and Covert 2009; Kean et al. 2011). Despite their ubiquity in these settings where they are the primary geomorphic response to fire, runoff-initiated debris flows are not common in the Pacific Northwest; only one instance of a runoff-initiated debris flow has been documented in the Eastern Cascades in Washington State (Klock and Helvey 1976; Helvey 1980; Wondzell and King 2003; Cannon and Gartner 2005; Parise and Cannon 2012). By contrast, shallow landslides initiated via soil saturation and root strength decline are the predominant geomorphic response to fire that is typical in the Pacific Northwest (Ziemer and Swanston 1977; McNabb and Swanson 1990; Schmidt et al. 2001; Jackson and Roering 2009; Lanini et al. 2009). As a result, the potential role and impact of post-fire runoff debris flows have not been addressed in western Oregon and Washington (Wondzell and King 2003).

The initiation of debris flows via runoff is promoted by high fire severity that dramatically alters the infiltration capacity of soil (Dryness 1976; DeBano et al. 1998; Cannon 2001; Huffman et al. 2001; Cannon and Gartner 2005; Woods and Balfour 2008; Doerr et al. 2009; Larsen et al. 2009; Mataix-Solera et al. 2011; Neris et al. 2013) combined with high-intensity rain, which results in rill and sheetwash erosion (Moody and Ebel 2012; Neary et al. 2012; Vieira et al. 2015; Gould et al. 2016; Robichaud et al. 2016). Runoff-initiated debris flows occur in response to immediate post fire reductions in soil infiltration rates and can therefore occur as soon as the first rainstorm that puts out the fire (e.g. Kean et al. 2019) or within a timeframe of days to years after a fire (Martin and Moody 2001; Moody and Martin 2001; Wondzell and King 2003; Cannon et al. 2008). The majority of runoff-initiated debris flows occur within 2 years after a fire and their likelihood declines rapidly as vegetation regenerates and hydrophobicity decreases (Doerr et al. 2000; Kean et al. 2011; Santi and Morandi 2013; Vieira et al. 2015). The transition between rilling and sheetwash into a debris flow depends heavily on topographic influences such as slope steepness, topographic convergence, and channel incision (Meyer and Wells 1997; Cannon et al. 2001).

In the Pacific Northwest, post-fire debris flows that result from shallow landslides have been previously documented (Roering et al. 2003; Woodsmith et al. 2004; Woodsmith et al. 2007; Jackson and Roering 2009; Lanini et al. 2009; Slesak et al. 2015), but the role of runoff-initiated debris flows in the region is not well understood. Wondzell and King (2003) suggest that runoff-initiated debris flows have only been documented in the Rocky Mountains, Interior Northwest, and southern California because of the prevalence of high-intensity rainfall bursts in these regions (Kean et al. 2011; Kampf et al. 2016). In the Pacific Northwest, long-duration, low-intensity rainfall paired with notably high soil infiltration rates makes the occurrence of runoff-initiated debris flows less likely (Dryness 1969; Harr 1977; McNabb et al. 1989; Schmidt 1995). Additionally, the effectiveness of hydrophobicity decreases with increased soil moisture (Wells et al. 1979), and soils in the Pacific Northwest tend to have higher soil moisture content than interior regions (Wondzell and King 2003). Therefore, in the Pacific Northwest's wet climate, high-intensity storm events typically do not result in runoff-initiated debris flows because they often encounter wet soils where the effects of hydrophobicity are reduced. Vegetative types also vary between the

Published online: 01 April 2020

Pacific Northwest and Interior Regions; Wondzell and King (2003) speculate that the rapid regeneration of vegetation after fire decreases the likelihood of runoff-initiated debris flows in this region.

On 20 June 2018, a runoff-initiated debris flow occurred in the Western Cascades in Oregon on the northwest flank of Black Crater. The debris flow occurred in a region that had burned 1-year prior during the 2017 Milli fire. This is the first reported case of a runoff-initiated debris flow occurring in the western, forested region of the Pacific Northwest, including regions such as the Western Cascades and Oregon Coast Range. We identified the Milli debris flow (MDF), to be initiated by surface runoff due to the observation of rills and sheetwash at the initiation zone (Wells 1987; Spittler 1995; Cannon et al. 2001). The objective of this paper is to provide a detailed characterization of this post-fire debris flow and to explore the conditions that facilitated this process to occur in the Pacific Northwest. As the effects of climate change result in more extreme wildfire events in the Pacific Northwest (Westerling et al. 2006; Gould et al. 2016), this region could become more susceptible to runoff-initiated debris flows.

Study area

Post-fire geomorphic processes in Western Oregon

Post-fire reductions in infiltration along with hydrophobicity have been observed in the Pacific Northwest (Dryness 1976; Johnson and Beschta 1980; DeBano 1981; McNabb et al. 1989; Jackson and Roering 2009). Despite this, runoff-initiated debris flows have not been observed because low-intensity rainfall characteristic of the Pacific Northwest rarely exceeds post-fire infiltration rates (McNabb et al. 1989; Schmidt 1995; Montgomery et al. 1997; Montgomery and Dietrich 2002; Wondzell and King 2003). For example, Schmidt (1995) found that post-wildfire change in soil infiltration was negligible in a watershed in southern Oregon for 2 years following fire due to high infiltration rates. McNabb et al. (1989) measured post-fire soil infiltration rates in the Oregon Coast Range using a mini-disk infiltrometer, finding infiltration rates to be significantly lower for burned soils rather than unburned, but these rates still exceeded rainfall rates by 2 to 3 times.

2018 Milli debris flow

The Milli debris flow occurred on 20 June 2018, on the northwest flank of Black Crater (Fig. 1). The debris flow began in a zone of dispersed rilling and sheetwash erosion on the upper slopes of Black Crater (Fig. 2a) and followed a path of subtle convergence until crossing Highway 242 in two locations at the toe of the slope (Fig. 2c–f). The June 20 storm event that triggered the debris flow had peak rainfall rates at 2:25 p.m. followed by another pulse at 4:00 p.m.

Geologic background and topography

Black Crater (~ 600-m relief) is a Pleistocene shield volcano and therefore has a broad, conical, gently sloping shape (Williams 1944). Convergence exists locally on Black Crater from minor dissection and stream network development (Fig. 3). The volcano is located on top of the undulating volcanic plateau of the Oregon High Cascades. Black Crater is an older volcano for the region and was glaciated during the last ice age (Williams 1944). In contrast to many of the younger volcanoes on the plateau, Black Crater is forested and has developed soils on its flanks. We identified the soils on Black Crater to be andisols that are fine-grained sandy loam. Tephra sourced from nearby volcanic activity composes much of the soil mantle.

Climate and vegetation

The annual precipitation in the Oregon Cascades is 3.5–4 m, and the climate is characterized by long-duration, low-intensity rainfall, which rarely exceeds forest soil infiltration rates even after intense fire (Wondzell and King 2003). Rapid regeneration of vegetation is characteristic of this wet climate, which further reduces the likelihood of runoff-initiated debris flows. East of the Cascades, precipitation declines to less than 0.4 m. Black Crater is positioned on this climatic divide. The eastern side of the mountain is vegetated by ponderosa pine (*Pinus ponderosa*) and bitterbrush (*Purshia tridentata*) woodland. The western flank of Black Crater is vegetated by Cascade Crest Montane Forest, which is dominated by mountain hemlock (*Tsuga mertensiana*) and pacific silver fir (*Abies alba*). The MDF initiated and flowed west through the Cascade Crest Montane Forest on Black Crater's northwest slope.

2017 Milli fire

The Milli fire began from a lightning strike on 11 August 2017, in the Three Sisters Wilderness within the fire boundary of the 2006 Black Crater Fire. The fire expanded into unburned fuel north of the boundary of the 2012 Pole Creek Fire and south of the 2006 Black Crater Fire. The Milli fire grew to be over 24,000 acres, resulting in the evacuation of homes in the area, and eventually was contained on 24 September 2017 (U.S. Forest Service 2017). The Burn Area Emergency Response team reported that 27% of the Milli fire area burned at moderate-to-high severities. We observed patches of severely burned soil at Black Crater, which were identifiable by their reddish-orange color. Further, 40% of the fire had greater than 50% overstory mortality, which also indicates a high-severity fire (U.S. Geological Survey 2017).

In 2018, the first summer after the Milli fire, revegetation was scarce to nonexistent and the soil was exposed, mixed with ash, charcoal, and pine needles. The burnt soil was very fine grained and dark gray in color. On the flank of Black Crater where the MDF occurred, 34% of the area was burned at low severity, 41% was burned at moderate severity, and 22% was burned at high severity (U.S. Geological Survey 2017; Fig. 4).

Methods

Field mapping

We mapped the debris flow initiation zone, runout, and the depositional area on the ground at the study site. At each source area and erosional observation, we measured and recorded the depths of erosional features. We defined the source area as the area where infiltration was in excess and rill erosion and sheetwash was observed. The erosional area was the area downslope of the source area with deeper erosional features. In addition, we mapped and measured the volume of the depositional area, using a metal probe to take 23 measurements of the deposit thickness.

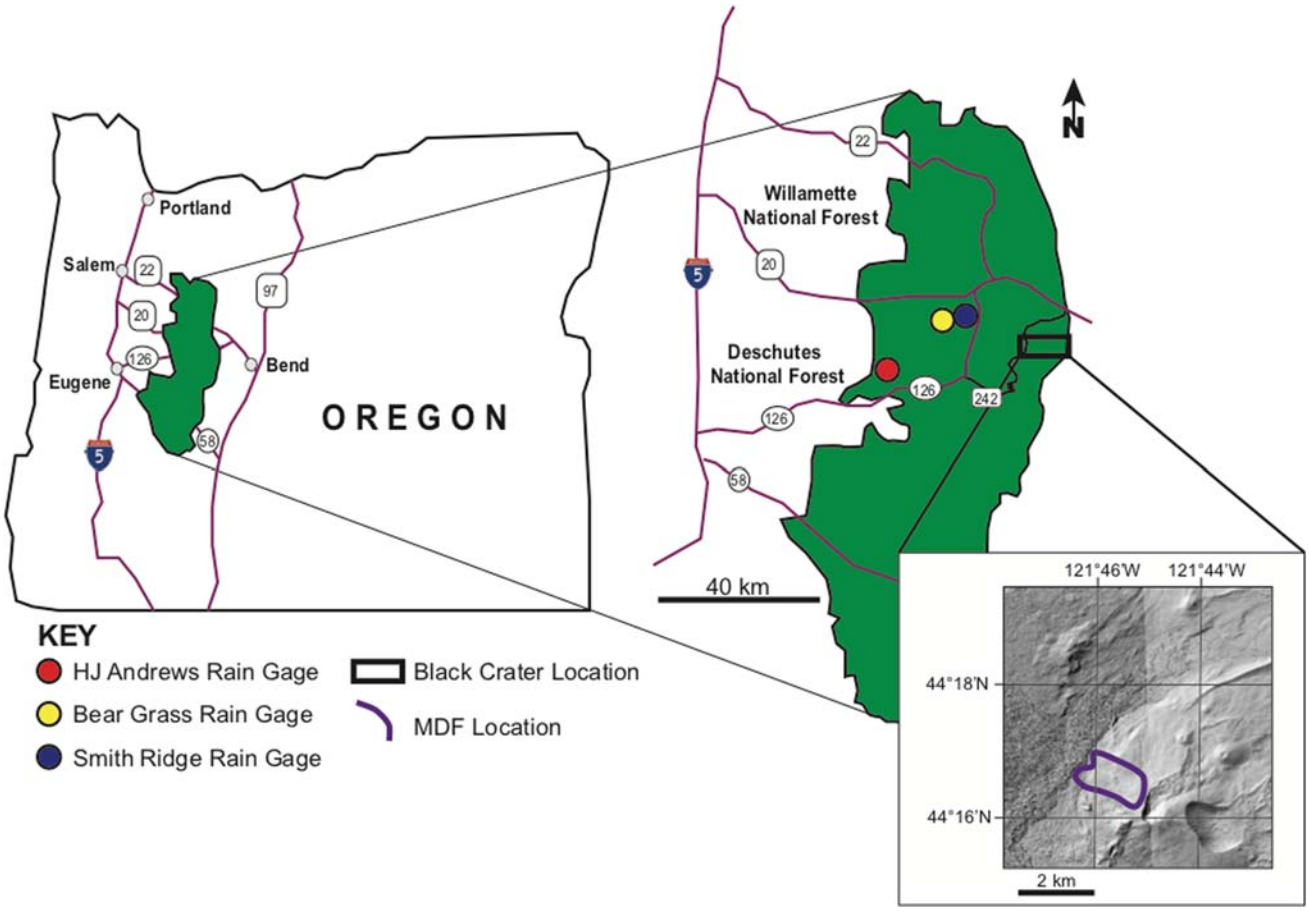

Fig. 1 Map showing location of Black Crater and nearby National Forests and highways, including geographic location of study site and the three rain gauges. The HJ Andrews rain gage is located at 44°13′N 122°14′W. Bear Grass Rain Gage is located at 44°20′N 122°6′W. Smith Ridge rain gage is located at 44°18′N 122°2′W

Soil infiltration rates

We used a mini-disk infiltrometer to estimate soil surface field-saturated hydraulic conductivity (Ks) (similar to McGuire et al. (2018)). We conducted measurements at nine different locations along the perimeter of the debris flow on soil surfaces that had been burned but not disturbed by the flow (Fig. 4). At each location, we conducted multiple measurements, which are labeled with their site location number and measurement number in Table 1. We measured soil infiltration rates at sites with variable burn severity, surface cover, and location on the hillslope (Table 1). The surface cover was predominantly pine needles at the sites. At these locations, we gently expressed air to clear needles away from the surface so that the mini-disk infiltrometer could properly make contact with the ground to form a suction.

Field measurements with the mini-disk infiltrometer were converted to Ks using the differentiated linearization method (DL) proposed by Vandervaere et al. (2000):

$$\frac{dI}{d\sqrt{t}} = C_1 + 2C_2\sqrt{t}, \tag{1}$$

where the I = cumulative infiltration rate, t = time, and C_1 and C_2 are fitting parameters. For each mini-disk measurement, the left hand side of Eq. 1 is solved numerically using measured infiltration at known time intervals and these values are plotted against the square root of the time measurement (e.g., $\sqrt{t}$). Equation 1 is a linear equation of the forms $y = mx + b$, where $y = \frac{dI}{d\sqrt{t}}$, $x = \sqrt{t}$, and C_1 and C_2 form the y-intercept (b) and slope (m) of the line, respectively. Subsequently, C_1 and C_2 are determined by fitting a best-fit line through the data points $y = \frac{dI}{d\sqrt{t}}$, $x = \sqrt{t}$, and finding C_1 and C_2 values that maximize the goodness of fit for the line. We can then use the fitted values of C_1 and C_2 to obtain soil hydraulic properties such as Sorptivity (S) and Ks using the relationships: $C_1 = A_1 S$ and $C_2 = A_2 K_s$. A_1 and A_2 are empirical constants, which can be determined using empirically derived equations (Zhang 1997):

$$A_1 = \frac{1.4b^{0.5}(\theta_0 - \theta_i)^{0.25}\exp[3(n-1.9)\alpha h_0]}{(\alpha r_0)^{0.15}} \tag{2}$$

$$A_2 = \frac{11.65(n^{0.1}-1)\exp[2.92(n-1.9)\alpha h_0]}{(\alpha r_0)^{0.91}} \text{ for } n \geq 1.9 \tag{3}$$

$$A_2 = \frac{11.65(n^{0.1}-1)\exp[7.5(n-1.9)\alpha h_0]}{(\alpha r_0)^{0.91}} \text{ for } n < 1.9 \tag{4}$$

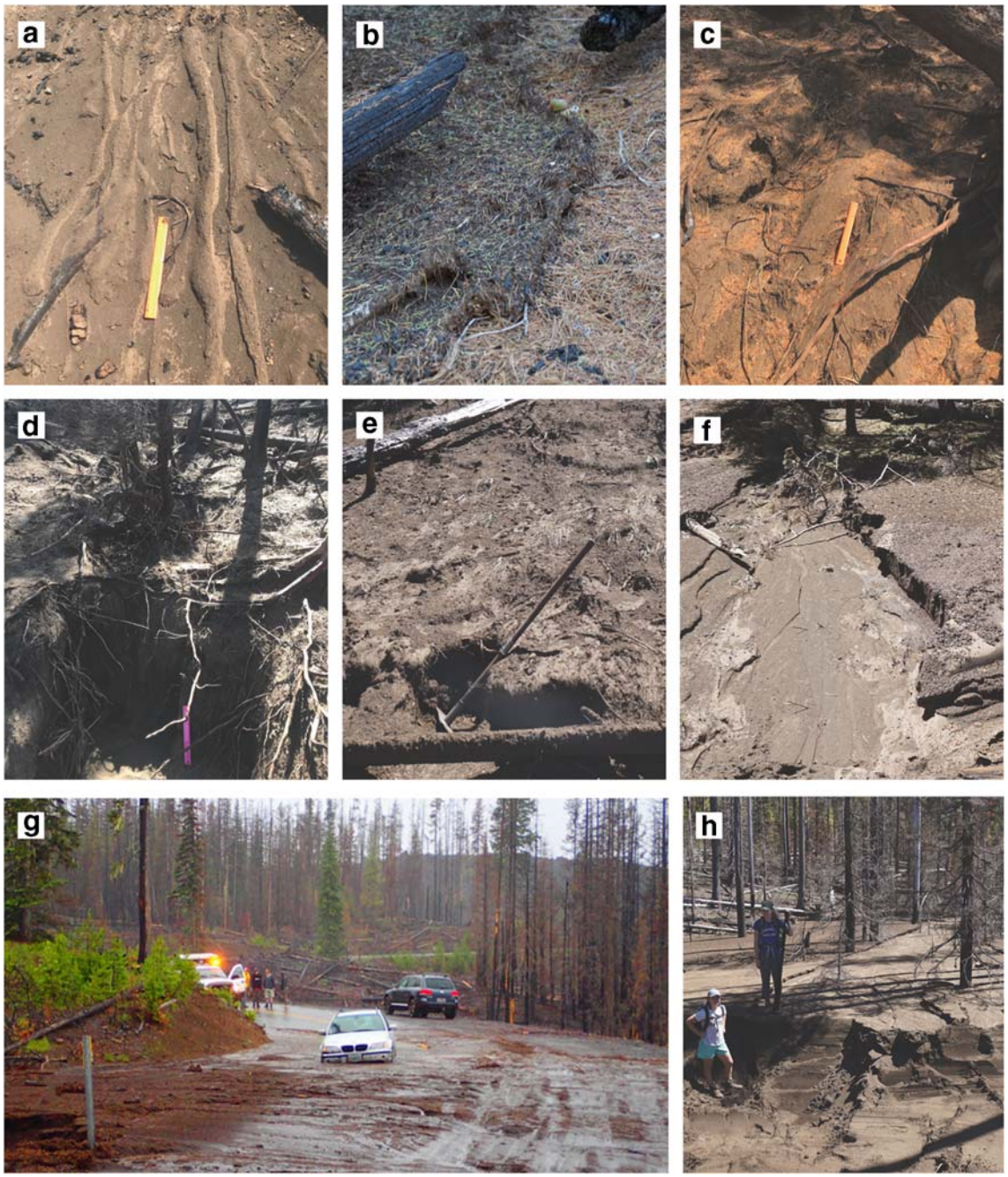

Fig. 2 **a** Photo of rills observed in the source area. **b** Levee on perimeter of flow composed of pine needles, charcoal, and fine sediments. **c** Erosional steps found along hillslope in the erosional area. **d** Deep channel (> 1 m depth) observed in the narrowest section of the flow. **e** Deeper channel in erosional area. **f** Wider, shallower channel observed in transition zone between erosional and depositional areas. **g** Photo taken on 20 June 2018 after the debris flow (O'Casey 2018). Shows the deposition washed across Highway 242. **h** Deposition upslope of Highway 242. Face of deposition visible due to bulldozer activity during highway clearing

where θ_o is the water content at the prescribed minidisk tension (h_o), θ_i is the initial water content (here, we assumed it was equal to the residual soil moisture θ_r), b is a fixed coefficient set to 0.55, and n and α are the van Genuchten parameters (van Genuchten 1980). We can determine the soil water content using the equation from Carsel and Parrish (1988) using

$$\theta_o = \theta_r - \frac{(\theta_s - \theta_r)}{(1 + (\alpha h_o)^n)^m} \quad (5)$$

where $m = 1 - 1/n$, and estimates of the saturated water content (θ_s) and residual (θ_r) were obtained using the US Department of Agriculture (USDA) Rosetta software (USDA 1999) (Table 2).

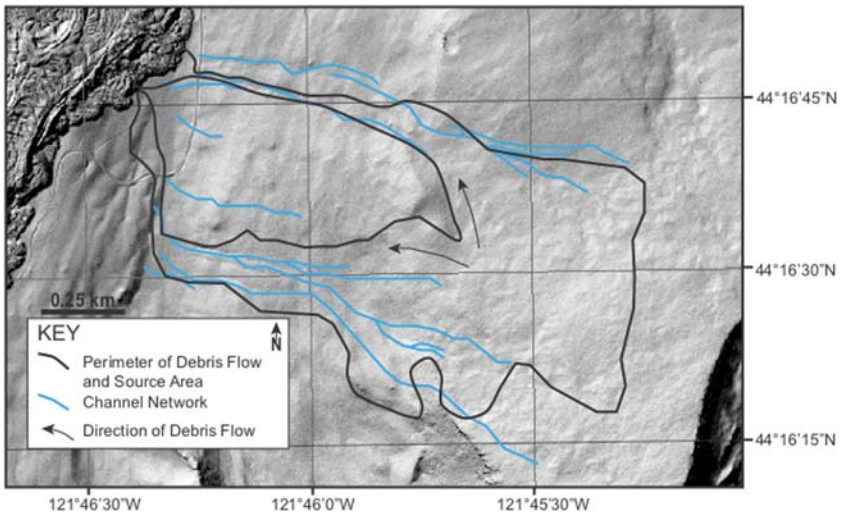

Fig. 3 LiDAR imagery of the northwest flank of Black Crater; blue lines indicate where water convergence exists on the volcano as determined through GIS analysis of the topography. The perimeter of the debris flow is layered on top of the GIS analysis for expected convergence and flow paths

Rosetta uses pedo-transfer functions to estimate hydraulic parameters based on the USDA soil textural classifications, in our case, a sandy loam. Additionally, we omitted the first measurement of each dataset to minimize any uncertainty in the temporal trend.

Rainfall analysis

To quantify the rainfall event that triggered the MDF, we obtained the rainfall data from three different gage locations (Fig. 1). Two of these sites were Snow Telemetry (SNOTEL) gages for the Natural Resources Conservation Service (NRCS) with hourly resolution, which use a fluid-based system relying on pressure transducers to estimate precipitation. From these data, we calculated hourly rainfall rates from September 2017 through September 2018. Because the gages are fluid-based sensors, however, the data are susceptible to diurnal air temperature fluctuations and barometric pressure changes, which necessitate adjustment. We chose to use rainfall data from the Bear Grass and Smith Ridge sites because of their proximity to the study area and because their data fluctuated less than other nearby sites (NRCS 2018a; NRCS 2018b). The Bear Grass gage is 10 km west of the study site and the Smith Ridge gage is 8 km west of the study site (Fig. 1). We used a third rainfall gage in the HJ Andrews Experimental Forest (located 40 km west of the study site (Daley 2018)). The data are from a meteorological station within the forest, which records rainfall at 5-min intervals. To compare these data to the SNOTEL sites, we converted the 5-min rainfall intensities into hourly intensities. We also calculated peak rainfall intensities for the storm event for 5-min, 15-min, 30-min, and 60-min intervals using the HJ Andrews rain gage data.

Results

Debris flow path characteristics

The MDF source area is characteristic of runoff-initiated debris flows observed in the literature. The source area is composed of an expansive, discontinuous network of rills that stretch 0.8 km across the slope and began just below Black Crater's summit, where slope angles vary from 11 to 30 degrees (Fig. 3). The rills are 1–4 cm deep (Fig. 5). We also observed evidence of sheetwash within the source area, which removed the top few centimeters of material from the hillslope. The sheetwash exposed shallow root networks but did not erode deeper than these structures.

The broad zone of rills and sheetwash in the source area transitioned to channelized flow downslope, coinciding with a local topographic convergence zone and a slope break. These topographic features contributed to the flow's evolution from rills and shallow channels into deeper eroded gullies, entraining sediment and forming the subsequent debris flow. Downslope of the slope break, deeper erosional features developed that coalesced into two channels that followed the valley networks on Black Crater's northwest face. Following the path of the valley networks, the debris flow converged to a width of 5 m at its most narrow point. Within the center of the channels, the erosional features were deeply eroded into the hillslope as uniform steps (Fig. 2c, d). The erosional channels had an average and maximum depth of 15 cm and 100 cm, respectively, and exposed roots and boulders (Fig. 2c, d). Splash lines from the debris flow were present on logs that had fallen perpendicular to the channel, revealing that during the event, flow depths exceeded 1.5 m. Along the perimeter of the flow, shallower and wider channels were present and lined with coarse levees between 1 and 4 cm tall composed of pine needles, charcoal, and fine sediments (Fig. 2b).

The debris flow began depositing sediment 80 m upslope of Highway 242, where slope steepness decreased and ranged between 0 and 10 degrees. The depositional area stretched across the highway and into the topographic depression below, where it was confined by a late Holocene lava flow. Post clearing of the road, we measured that the deposition was deepest (1.62 m) in the center of the flow upslope of the road and thinned greatly towards the edges. In total, 1.2×10^4 cubic meters of fine-grained, well-sorted dark gray sediment was deposited by the debris flows two paths.

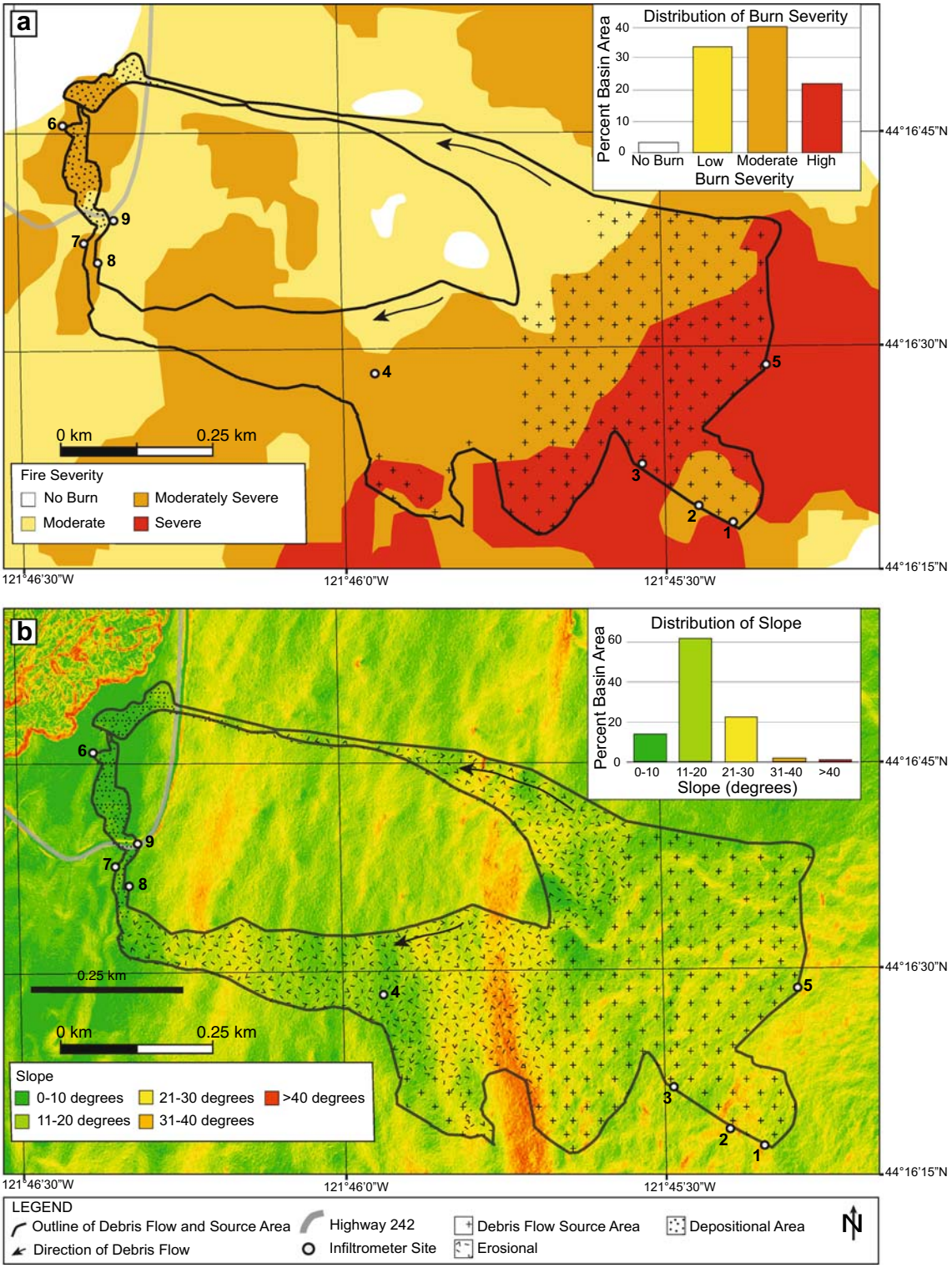

Fig. 4 **a** Map of relationship between fire severity and location of the MDF and debris flow features. Bar graph shows distribution of fire severities on the flank of Black Crater where the debris flow occurred. **b** Map of relationship between slope steepness and the location of the MDF and debris flow features. Bar graph shows the distribution of slope steepness on the flank of Black Crater where the debris flow occurred. Both maps show location of infiltrometer sites and features of the MDF

Fire severity

The entirety of the MDF occurred within the bounds of the Milli fire (Fig. 4). The source area of the MDF aligns with the patches of the forest that was burned with high severity. Additionally, 52% of the MDF source area occurred within the high-severity burn area, while the rest occurred directly downslope of these regions in

Table 1 Measurements of hydraulic conductivity (Ks), sorptivity (S), and site characteristics for each study site

Site	Measured Ks (mm/h)	Sorptivity ($mm/h^{0.5}$)	Burn severity	Location	Ground cover	Slope
1	n/a	n/a	Moderate	Source area	Pine needles	21–30 degrees
2.1	47.52	90.60	Moderate	Source area	Pine needles	21–30 degrees
2.2	25.63	20.39	Moderate	Source area	Pine needles	21–30 degrees
2.3	15.60	30.66	Moderate	Source area	Pine needles	21–30 degrees
2.4	20.23	n/a	Moderate	Source area	Pine needles	21–30 degrees
2.5	21.23	7.85	Moderate	Source area	Pine needles	21–30 degrees
3.1	131.90	141.65	High	Source area	No ground cover	21–30 degrees
4.1	n/a	13.10	Moderate	Erosional	Pine needles	11–20 degrees
4.2	25.49	60.42	Moderate	Erosional	Pine needles	11–20 degrees
4.3	14.37	64.41	Moderate	Erosional	Pine needles	11–20 degrees
4.4	21.17	56.72	Moderate	Erosional	Pine needles	11–20 degrees
4.5	37.96	27.86	Moderate	Erosional	Pine needles	11–20 degrees
5.1	12.86	87.30	High	Source area	Pine needles	21–30 degrees
5.2	36.62	83.09	High	Source area	Pine needles	21–30 degrees
5.3	50.81	107.53	High	Source area	Pine needles	21–30 degrees
6.1	47.32	119.35	Moderate	Depositional	Pine needles	0–10 degrees
6.2	3.78	124.68	Moderate	Depositional	Pine needles	0–10 degrees
6.3	114.42	37.91	Moderate	Depositional	Pine needles	0–10 degrees
6.4	59.82	n/a	Moderate	Depositional	Pine needles	0–10 degrees
6.5	n/a	n/a	Moderate	Depositional	Pine needles	0–10 degrees
7.1	30.68	n/a	Moderate	Erosional	Pine needles	11–20 degrees
7.2	54.20	n/a	Moderate	Erosional	Pine needles	11–20 degrees
7.3	46.60	n/a	Moderate	Erosional	Pine needles	11–20 degrees
7.4	72.52	3.18	Moderate	Erosional	Pine needles	11–20 degrees
7.5	129.55	n/a	Moderate	Erosional	Pine needles	11–20 degrees
8.1	0.17	19.75	Moderate	Erosional	Pine needles	11–20 degrees
8.2	9.38	n/a	Moderate	Erosional	Pine needles	11–20 degrees
8.3	6.26	24.80	Moderate	Erosional	Pine needles	11–20 degrees
8.4	2.94	13.94	Moderate	Erosional	Pine needles	11–20 degrees
8.5	n/a	31.19	Moderate	Erosional	Pine needles	11–20 degrees
9.1	61.26	n/a	Low	Depositional	Pine needles	0–10 degrees
9.2	38.84	n/a	Low	Depositional	Pine needles	0–10 degrees
9.3	4.48	15.80	Low	Depositional	Pine needles	0–10 degrees
9.4	47.74	n/a	Low	Depositional	Pine needles	0–10 degrees
9.5	36.01	n/a	Low	Depositional	Pine needles	0–10 degrees
Mean	39.59	53.74				
Geometric mean	23.61	36.53				

moderate severity burn areas. Everywhere within the MDF boundary that had been burned at high severity was observed to be a source area for the flow due to the presence of rill and sheetwash erosion.

Table 2 Hydraulic parameters estimated using the Rosetta software for a sandy loam soil

θ_s	0.3870 [–]
θ_r	0.0387 [–]
n	1.4484 [–]
α	0.0267 [cm^{-1}]

Soil infiltration rates

The measured saturated hydraulic conductivity within the study area had a geometric mean of 23.6 mmh^{-1} (Table 1). The data approximate a lognormal distribution and have a standard deviation of SD = 34.5 mmh^{-1} (Fig. 6). At sites 1, 2, and 3, fire severity ranged from moderately high to high severities and the slope averaged 21–30 degrees. The infiltration rates at these sites have a geometric mean of 32.0 mm h^{-1}. Additionally, the interquartile range for the sites in the source area is between 20.0 and 59.5 mmh^{-1} (Fig. 6). At sites 4,7, and 8, fire severity ranged from moderate to moderately high severities and slope averaged 11–20 degrees. Infiltration rates at these sites have a geometric mean of 16.4 mmh^{-1}. Additionally, the interquartile range for the sites in the source area is between 6.4 and 46.4 mmh^{-1} (Fig. 6). Lastly, infiltrometer data for depositional sites 6 and 9 have a geometric mean of 30.4 mm h^{-1}, and the interquartile range for the sites in the source area is between 22.0 and 69.6 mmh^{-1} (Fig. 6). Generally, the sorptivity measured at the site was higher than has been observed in other burn areas (Ebel and Moody 2016), which may reflect the partial recovery of the soil hydraulic properties at the time of the infiltration measurements (Table 1).

Rainfall

From the rainfall data collected at the HJ Andrews Experimental Forest, Smith Ridge SNOTEL, and Bear Grass SNOTEL gages, we calculated rainfall rates for the storm event that triggered the debris flow and for storm events from the previous year. The rainfall rates that triggered the MDF on 20 June 2018 were unusually high compared to rainfall rates from previous storms in the 2017 to 2018 years between the Milli fire and the debris flow (Fig. 7). Additionally, the data revealed two distinct bursts of sustained, high-intensity rainfall during the June 20 storm event (Fig. 6).

The mean rainfall rate for the 2017 to 2018 year was 3.0 mmh^{-1}, and peak hourly rainfall rates for the June 20 storm event were 9.1 mmh^{-1}, 27.9 mmh^{-1}, and 27.9 mmh^{-1}, for the HJ Andrews, Bear Grass, and Smith Ridge rain gages, respectively. The HJ Andrews rain gage reported the first rain peak as 11.2 mm h^{-1} for 15 min at 2:25 p.m. This was followed by the second peak of 25.4 mm h^{-1} at 4:05 p.m. (Fig. 6). Over the course of the storm, 2.8 mm of rain fell during the first burst and 9.4 mm of rain fell during the second burst at HJ Andrews, resulting in a total of 12.2 mm of rainfall at the gage over the course of the storm. The peak rainfall intensities at the HJ Andrews rain gage were 25.4 mm h^{-1} (5 min), 21.3 mm h^{-1} (15 min), and 16.3 mm h^{-1} (30 min) (Fig. 8).

Discussion

Our results suggest that the combination of high-severity fire, high-intensity rainfall, topographic convergence and steepness,

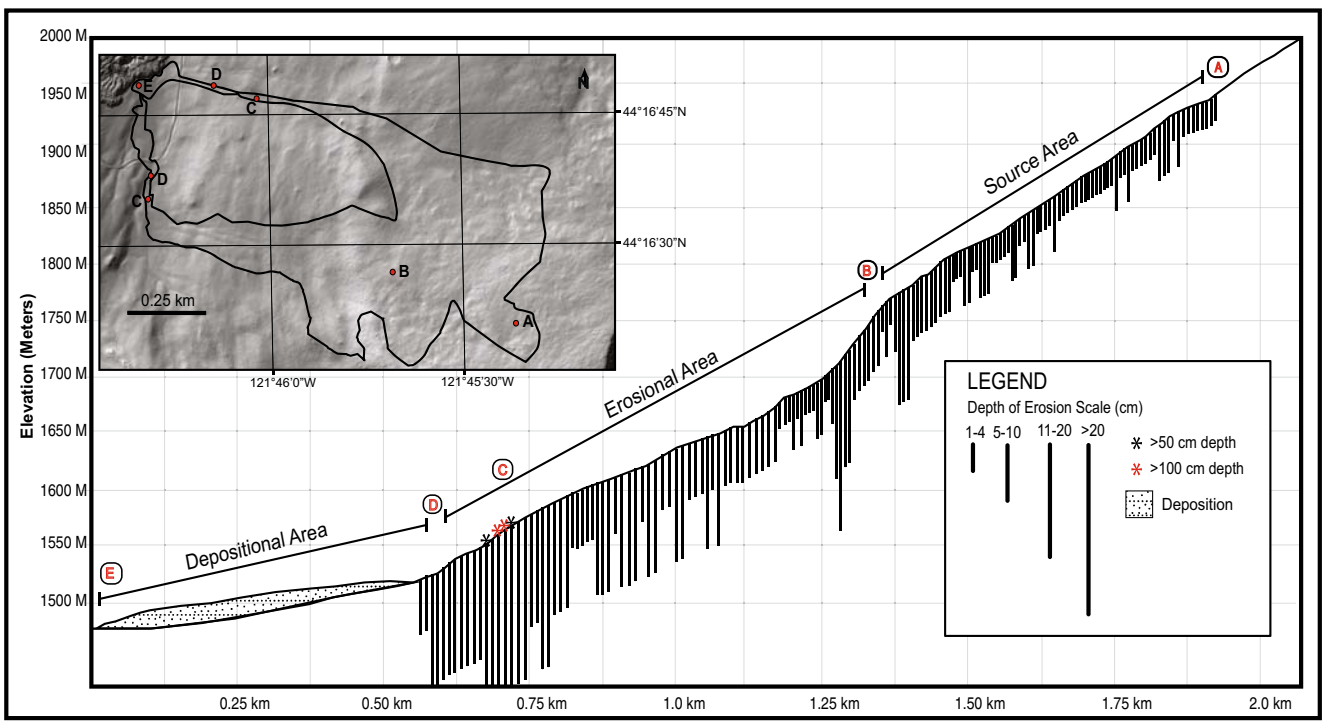

Fig. 5 Shows longitudinal profile of erosional depths along the hillslope. The cross section follows two paths: one from A to E along the north channel network and one from A to E along the southern channel network. Erosional depths are a compilation of data from both channel networks. A marks the upper limit of the source area, B marks the transition between source area and erosional features, C marks toe of slope where erosional features are deepest, D marks transition between erosional and depositional zones, and E marks the end of the depositional area. Vertical exaggeration of 5×

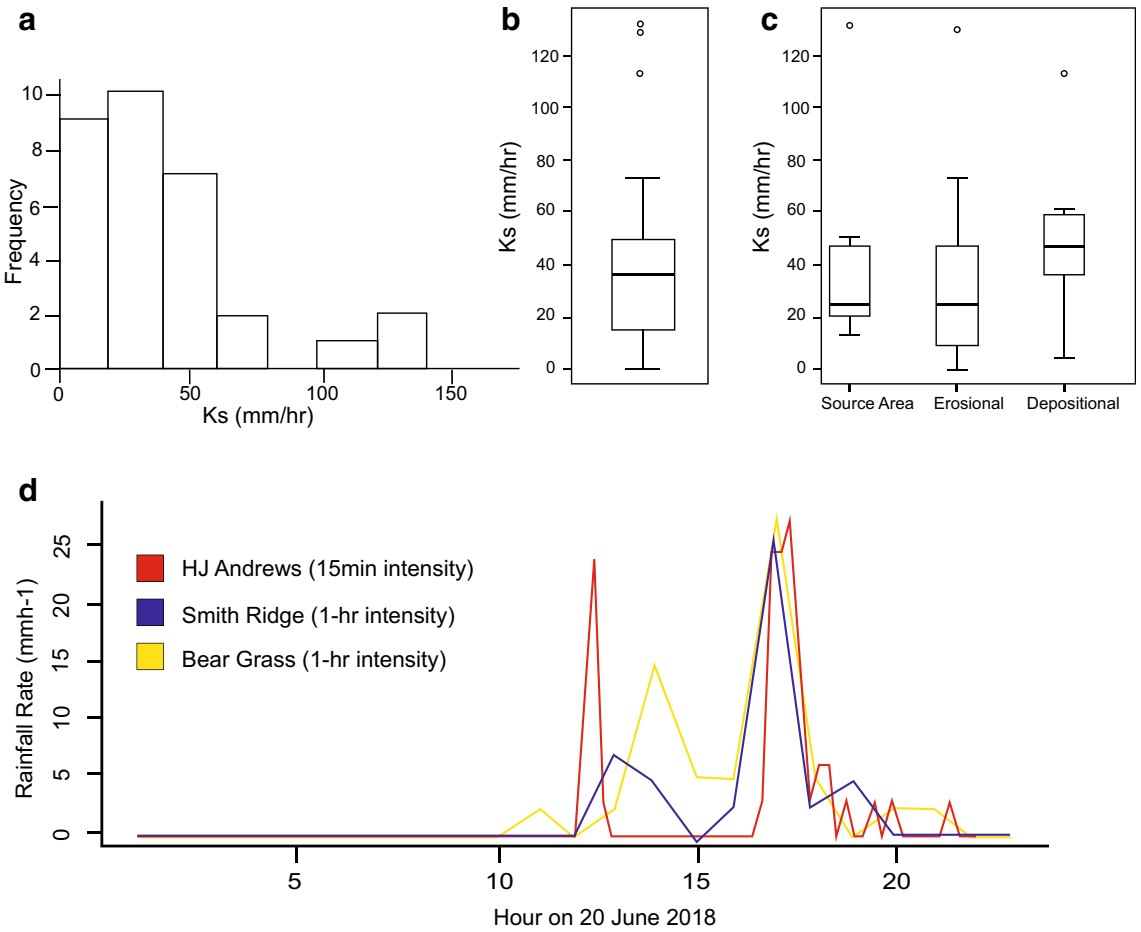

Fig. 6 **a** Distribution of infiltration rates. **b** Boxplot distributions of all infiltrometer sites. **c** Spatial boxplot distributions of infiltration rates at source area, erosional area, and depositional area. **d** Graph shows hourly rainfall rates for the three rain gauges during the June 20, 2018 storm event. The time count begins at 12:00 a.m. on 20 June 2018

and ample soil mantle on the flanks of Black Crater combined to initiate the MDF. The MDF followed patterns observed in the literature regarding fire severity, source area erosion, soil characteristics, and rainfall event (Meyer and Wells 1997; Cannon et al. 2001; Wondzell and King 2003; Cannon and Gartner 2005). In addition, the conical and divergent topography of Black Crater is distinct from most catchments in the literature where other runoff-initiated debris flows have been observed (Cannon et al. 2001; Cannon and Gartner 2005; Staley et al. 2017).

The area of a hillslope burned at moderate to high severities is one of the most influential factors whether a debris flow is initiated (Cannon and Gartner 2005; Doerr et al. 2006; Cannon et al. 2010; Gould et al. 2016). Of the 24 runoff-initiated debris flows studied by Kean et al. (2011), 91% of debris flows were initiated from basins with more than 65% of their areas burned at moderate to high severities (Cannon and Gartner 2005). At the MDF study site, 63% of the area was burned at moderate to high severities, and it is notable that 100% of the source area for the MDF was burned at moderate to high severities (Fig. 4). This suggests that overland flow was initiated on the hillslope in areas where the soil was most influenced by fire and therefore where soil infiltration capacity was most reduced.

The Milli fire that burned Black Crater in 2017 is noted as the highest-severity fire of the 2017 Oregon fire season (U.S. Forest Service 2017). This fire fits into a broader trend of increasing frequency of high severity fires in the Pacific Northwest due to climate change (Westerling et al. 2006; Wimberly and Liu 2014; Gould et al. 2016). The 2017 fire season in Oregon was marked by extreme fire behavior of multiple large, long-duration fires and has been recognized as the worst, and one of the longest, fire seasons on record in the state (U.S. Forest Service 2017; Oregon Forest Resources Institute 2018). This pattern has been observed in interior British Columbia (BC), Canada, where debris flows initiated via shallow-landsliding were the primary post-fire response in the region due to high soil infiltration rates and low rainfall intensities (Jordan and Covert 2009). After the 2003 fire season, which was recognized as the most severe on record in BC at the time, post-fire debris flows initiated via runoff were observed in multiple locations in the region (Jordan and Covert 2009). Since the 2003 fire season, post-fire, runoff-initiated debris flows have continued to be observed in interior BC (Jordan 2014). As high-severity fires increase in frequency in the Pacific Northwest, this region could begin to experience more frequent runoff-initiated, post-fire debris flows in the future.

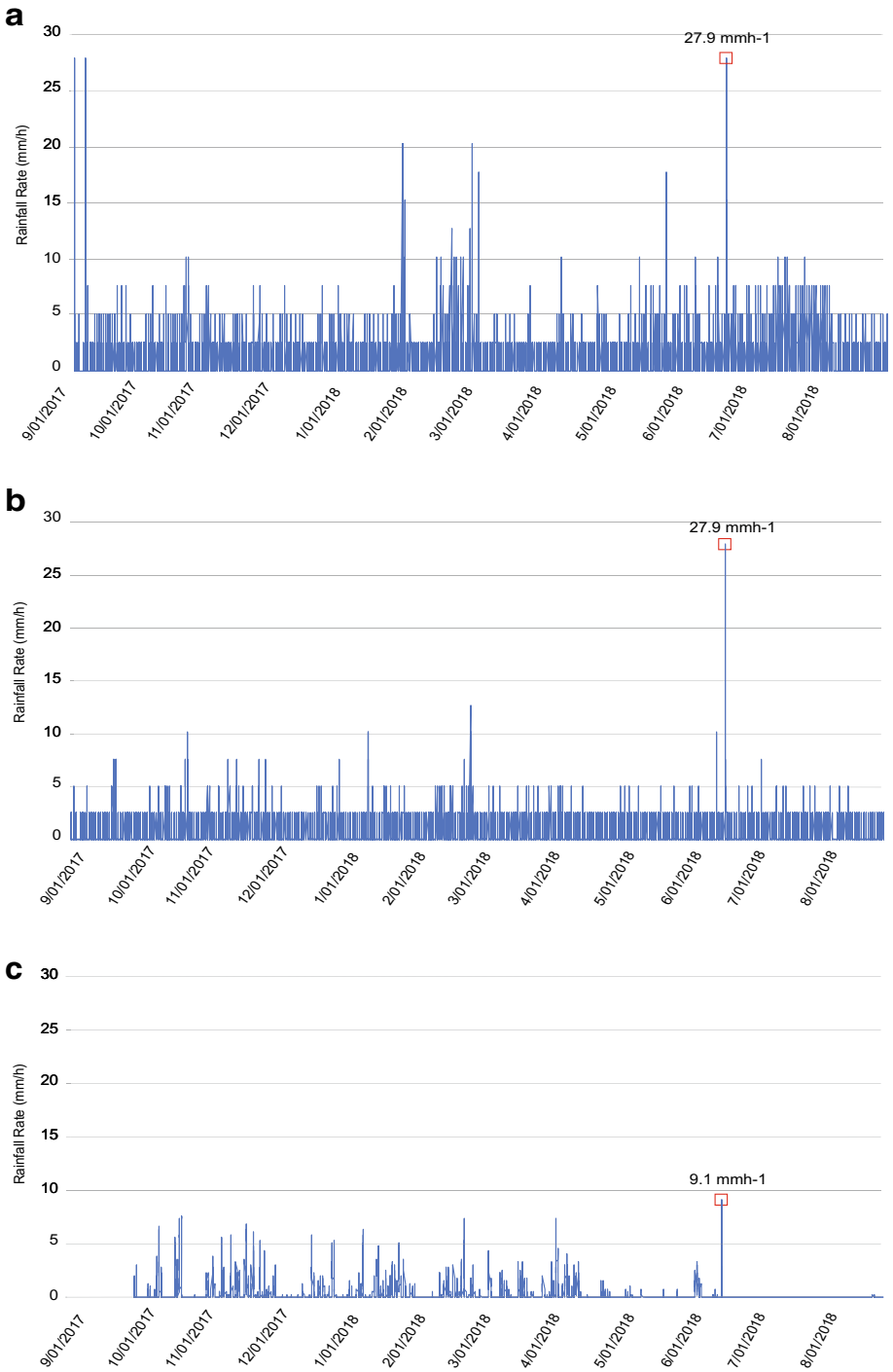

Fig. 7 Graphs show rainfall intensities between 1 Sept. 2017 to 1 Sept. 2018, which is the year between the occurrence of the Milli Fire and the debris flow. **a** Rainfall at Bear Grass SNOTEL site. **b** Rainfall at Smith Ridge SNOTEL site. **c** Rainfall at HJ Andrews Experimental Forest site

While infiltration-excess overland flow does not typically occur in the Pacific Northwest due to the prevalence of low-intensity rainfall and notably high infiltration rates, the infiltration rates observed at the study site were significantly lower than previously documented infiltration rates in the Pacific Northwest (Montgomery et al. 1997; Montgomery and Dietrich 2002). In previous studies conducted in the Western Oregon Cascades, infiltration rates were found to range from 80.0 mmh^{-1} to over 200 mmh^{-1} (U.S. Forest Service 1973; Johnson and Beschta 1980; Johnson and Beschta 1981). In contrast, at Black Crater, the observed infiltration rates had a mean of 39.6 mm h^{-1} and a geometric mean of 23.6 mm h^{-1} with high variation. Variability observed in the measured infiltration rates could indicate differences in fire severity, soil moisture, or hydrophobicity at different locations on the hillslope.

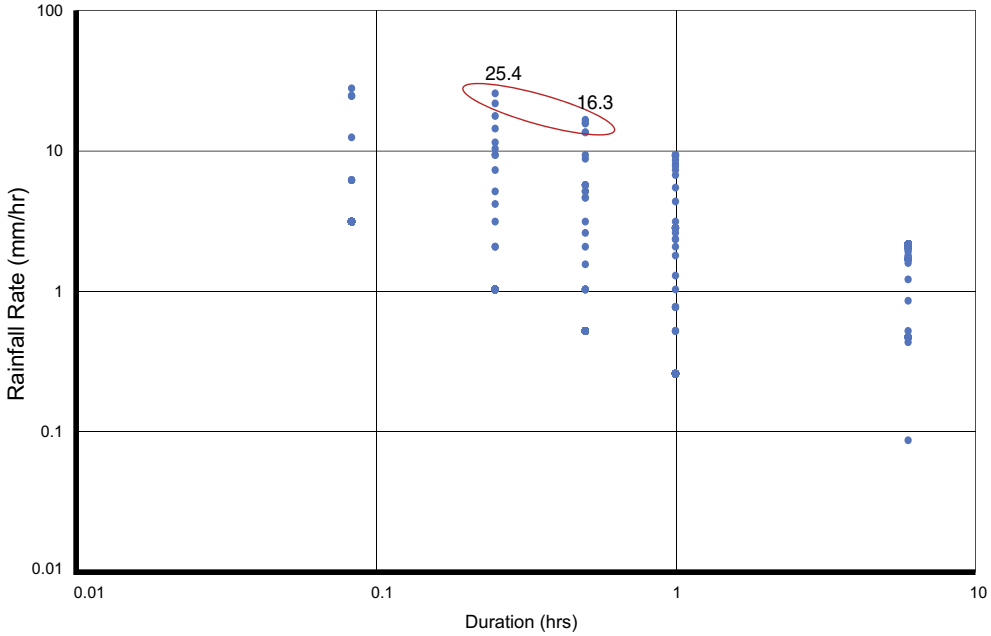

Fig. 8 Graph shows intensity-duration data for the rainfall rates recorded at HJ Andrews site during the June 20 storm event. The red ellipse is around peak 15-min and 30-min rainfall rates, all of which exceeded 15 mmh^{-1} for the designated time interval. Shows that high-intensity rainfall was sustained for 15- to 30-min intervals at this site

The infiltration rates observed at the study site were likely to be biased towards higher values for numerous reasons. First, the infiltration data were collected from soil surfaces in areas adjacent to the flow that did not initiate the debris flow or become incorporated into the flow. Areas in which the flow initiated or eroded could have had lower infiltration rates than the surfaces from which we collected the data. Additionally, the soil infiltration rate measurements were taken after the storm event that triggered the debris flow, which means soil moisture content was likely higher during our measurements than before the storm event. Thus, it is possible the effects of hydrophobicity were reduced when our measurements were taken.

The storm event that triggered the MDF had relatively high but not uncommon rainfall intensity for the 2017–2018 year (Fig. 7). The magnitude of this storm event has a return interval of 2 to 5 years (Oregon Department of Transportation 2014). The June 20 storm event was the first large storm of the summer, which means that this intense rainfall would have fallen on dry soil when hydrophobicity is most effective. There is uncertainty in the rainfall data because the rain gage locations range from 10 to 40 km away from the study site. Further, the HJ Andrews gage, Smith Ridge gage, and Bear Grass gage are located at elevations of 1280 m, 997 m, and 1438 m, respectively. In contrast, the MDF was initiated on Black Crater at an elevation of 1950 m and was located at the crest of the Cascades. There may have been an orographic effect creating higher rainfall intensities at Black Crater than recorded by the rain gages, but no supporting data are available closer to the study location. Nonetheless, the rainfall rates during the storm event were on the same order of magnitude as the infiltration rates observed at Black Crater. Interpretation of Fig. 8 reveals that at HJ Andrews, rainfall intensities of 25.4 mmh^{-1} exceeded the geometric mean of measured Ks (23.6 mmh^{-1}) at the study site for a duration of 15 min.

While rainfall intensities reported during the June 20 rain event are generally lower than the average infiltration rates observed across the study area, there is wide spatial variability in the infiltration rate data (Fig. 6). This suggests that there are localized patches across the hillslope of lower infiltration rates as has been observed at other burned sites in the Pacific Northwest (Jackson and Roering 2009). Additionally, towards the summit, where the source area is located, the soil becomes thinner and in situ bedrock is visible. In these places where soil is thin or nonexistent, infiltration is negligible and infiltration-excess overland flow is favored. The observed patches of low infiltration rates paired with field observations of rill erosion and sheetwash together support the theory that infiltration-excess overland flow occurred at Black Crater during the June 20 rain event.

Conclusion

This study offers evidence that infiltration-excess overland flow resulted in a debris flow on the flanks of Black Crater on 20 June 2018. The combination of high severity fire, reduced infiltration rates, and a 2- to 5-year interval storm event resulted in the occurrence of the MDF. Our findings suggest that high fire severity dramatically reduced infiltration rates at the study site, which are significantly lower than infiltration rates observed at other locations in western Oregon. Rainfall rates during the storm event were similar to infiltration rates observed at the site, consistent with observations that infiltration-excess overland flow occurred at this location. Despite the broad, conical shape of Black Crater, subtle convergence, and steep slopes promoted the transition between source area rilling and sheetwash to a fully mobilized debris flow.

As fire seasons lengthen and fire intensity increases across the Pacific Northwest as a result of climate change, this region may become more susceptible to runoff-initiated debris flows. Our results shed light on conditions conducive to runoff-initiated debris flows in the Pacific Northwest, improving our ability to forecast post-fire, runoff-initiated debris flows in the future.

Acknowledgments

This research has been supported by the Kolenkow-Reitz Fellowship through Carleton College. We thank the editors for their insight and helpful comments on the manuscript. Reviews by Mary Savina throughout the process were very constructive and greatly appreciated. We also thank members of the University of Oregon Earth Surface Processes Lab for their invaluable contributions to the fieldwork. Any use of trade, firm, or product names is for descriptive purposes only and does not imply endorsement by the U.S. Government. Data will be made available in the University of Oregon Scholar's Bank.

References

Cannon S (2001) Debris-flow generation from recently burned watersheds. Environ Eng Geosci 7:321–341. https://doi.org/10.2113/gseegeosci.7.4.321

Cannon S, Bigio E, Mine E (2001) A process for fire-related debris flow initiation, Cerro Grande fire, New Mexico. Hydrol Process 15:3011–3023. https://doi.org/10.1002/hyp.388

Cannon S, Gartner J (2005) Wildfire-related debris flow from a hazards perspective. Debris-flow Hazards and Related Phenomena. Springer Praxis Books, In, pp 363–385. https://doi.org/10.1007/3-540-27129-5_15

Cannon S, Gartner J, Wilson R, Bowers J, Laber J (2008) Storm rainfall conditions for floods and debris flows from recently burned areas in southwestern Colorado and southern California. Geomorphology 96:250–269

Cannon SH, Gartner JE, Rupert MG, Michael JA, Rea AH, Parrett C (2010) Predicting the probability and volume of postwildfire debris flows in the intermountain western United States. Geol Soc Am Abstr Programs 122(1-2):127–144

Carsel RF, Parrish RS (1988) Developing joint probability distributions of soil water retention characteristics. Water Resour Res 24(5):755–769

Daley C (2018) Primet 230 a 5min 2018, Andrews Forest Long Term Ecological Research. https://andrewsforest.oregonstate.edu/sites/default/files/lter/data/weather/portal/PRIMET/data/primet_230_a_5min_2018.html

DeBano L (1981) Water repellent soils: a state-of-the-art. Pacific Southwest Forest and Range Experimental Station General Technical Report 46

DeBano L, Neary D, Ffolliott P (1998) Physical soil system. In: Fire's effects on ecosystems. Wiley, New York, pp 84–102

Doerr H, Shakesby R, Walsh R (2000) Soil water repellency–its causes, characteristics and hydro geomorphological significance. Earth Sci Rev 51:33–65

Doerr SH, Shakesby RA, Blake WH, Chafer CJ, Humphreys GS, Wallbrink PJ (2006) Effects of differing wildfire severities on soil wettability and implications for hydrological response. J Hydrol 319:295–311

Doerr S, Shakesby R, MacDonald L (2009) Soil water repellency-a key factor in post-fire erosion?. In: Fire effects on soils and restoration strategies. CRC Press, Boca Raton, p 28

Dryness C (1969) Hydrologic properties of soils on three small watersheds in the Western Cascades of Oregon. USDA For Ser Res Paper PNW-111:17

Dryness C (1976) Effects of wildfire on soil wettability in the high Cascades of Oregon. USDA for. Ser. Res. Paper PNW-202

Ebel BA, Moody JA (2016) Synthesis of soil-hydraulic properties and infiltration time-scales in wildfire-affected soils. Hydrol Process 31:324–340

Gould GK, Liu M, Barber ME, Cherkauer KA, Robichaud PR, Adam JC (2016) The effects of climate change and extreme wildfire events on runoff erosion over a mountain watershed. J Hydrol 536:74–91

Harr R (1977) Water flux in soil and subsoil on a steep forested slope. J Hydrol 33:37–58

Helvey J (1980) Effects of a North Central Washington wildfire on runoff and sediment production. J Am Water Resour Assoc 16:627–634

Huffman E, MacDonald L, Stednick J (2001) Strength and persistence of fire-induced soil hydrophobicity under ponderosa and lodgepole pine, Colorado front range. Hydrol Process 15:2877–2892

Inbar M, Tamir M, Wittenberg L (1998) Runoff and erosion processes after a forest fire in Mount Carmel, a Mediterranean area. Geomorphology 24:17–33

Jackson M, Roering J (2009) Post-fire response in steep, forested landscapes: Oregon coast range, USA. Quat Sci Rev 28:1131–1146

Johnson M, Beschta R (1980) Logging, infiltration capacity, and erodibility in Western Oregon. J For 78:6

Johnson M, Beschta R (1981) Seasonal variation of infiltration capacities of soils in Western Oregon. USDA Forest Service Research Note PNW-373

Jordan P (2014) Post-wildfire debris flows in southern British Columbia, Canada. Int J Wildland Fire 25:322–336

Jordan P, Covert A (2009) Debris flows and floods following the 2003 wildfires in southern British Columbia. Environ Eng Geosci 15:217–234

Kampf SK, Brogan DJ, Schmeer S, MacDonald LH, Nelson PA (2016) How do geomorphic effects of rainfall vary with storm type and spatial scale in a post-fire landscape? Geomorphology 273:39–51

Kean J, Staley D, Cannon S (2011) In situ measurements of post-fire debris flows in southern California: comparisons of the timing and magnitude of 24 debris-flow events with rainfall and soil moisture conditions. J Geophys Res 116

Kean JW, Staley DM, Lancaster JT, Rengers FK, Swanson BJ, Coe JA, Hernandez JL, Sigman AJ, Allstadt KE, Lindsay DN (2019) Inundation, flow dynamics, and damage in the 9 January 2018 Montecito debris-flow event, California, USA: Opportunities and challenges for post-wildfire risk assessment. Geosphere 15(X):1–24. https://doi.org/10.1130/GES02048.1

Klock G, Helvey J (1976) Soil-water trends following wildfire on the Entiat Experimental Forest [Washington]. Proceedings Tall Timbers Fire Ecology Conference, pp 193-200

Lanini JS, Clark EA, Lettenmaier DP (2009) Effects of fire-precipitation timing and regime on post-fire sediment delivery in Pacific northwest forests. Geophys Res Lett 36

Larsen I, MacDonald L, Brown E, Rough D, Welsh M, Pietraszek J, Libohova Z, Juan S (2009) Causes of post-fire runoff and erosion: water repellency, cover, or soil sealing? Soil Sci Soc Am J 73:1393

Martin D, Moody J (2001) Comparison of soil infiltration rates in burned and unburned mountainous watersheds. Hydrol Process 15:2893–2903

Mataix-Solera J, Cerdà A, Arcenegui V, Jordán A, Zavala L (2011) Fire effects on soil aggregation: a review. Earth Sci Rev 109:44–60

McGuire L, Rengers F, Kean J, Staley D (2018) Incorporating spatially heterogeneous infiltration capacity into hydrologic models with applications for simulating post-fire debris flow initiation. Hydrol Process 32:1173–1187

McNabb D, Swanson F (1990) Effects of fire on soil erosion. In: Natural and Prescribed Fire in Pacific Northwest Forests USDA For Ser Res Paper 1978:159–176

McNabb D, Gaweda F, Froehlich H (1989) Infiltration, water repellency, and soil moisture content after broadcast burning in a forest site in Southwest Oregon. J Soil Water Conserv 44:87–90

Meyer G, Wells S (1997) Fire-related sedimentation events on alluvial fans, Yellowstone National Park, USA. J Sed Res 67:5

Montgomery D, Dietrich W (2002) Runoff generation in a steep, soil-mantled landscape. Water Resour Res 38:1168

Montgomery D, Dietrich W, Torres R, Anderson SP, Heffner J, Loague K (1997) Hydrologic response of a steep, unchanneled valley to natural and applied rainfall. Water Resour Res 33:91–109

Moody J, Ebel B (2012) Hyper-dry conditions provide new insights into the cause of extreme floods after wildfire. Catena 93:58–63

Moody JA, Martin DA (2001) Initial hydrologic and geomorphic response following a wildfire in the Colorado front range. Earth Surf Process Landf 26:1049–1070

Neary D, Koestner K, Youberg A, Koestner P (2012) Post-fire rill and gully formation, Schultz fire 2010, Arizona, USA. Geoderma 191:97–104

Neris J, Tejedor M, Fuentes J, Jiménez C (2013) Infiltration, runoff and soil loss in Andisols affected by forest fire (Canary Islands, Spain). Hydrol Process 27:2814–2824

NRCS (2018a) Bear grass. Natural Resources Conservation Service: https://wcc.sc.egov.usda.gov/nwcc/site?sitenum=1166

NRCS (2018b) Smith ridge. Natural Resources Conservation Service: https://wcc.sc.egov.usda.gov/nwcc/site?sitenum=1167

O'Casey T (2018) Storms spark C.O. fires, send mud across Hwy. 242. News Channel 21: https://www.ktvz.com/news/storms-spark-wildfires-send-mud-across-hwy-242/756105316

Oregon Department of Transportation (2014) ODOT Hydraulics Manual. chapter 7, Appendix A: https://www.oregon.gov/ODOT/GeoEnvironmental/Docs_Hydraulics_Manual/Hydraulics-07-A.pdf

Oregon Forest Resources Institute (2018) Impacts of Oregon's 2017 wildfire season. OFRI Wildfire Report-Final 1/2/18. https://oregonforests.org/sites/default/files/2018-01/OFRI%202017%20Wildfire%20Report%20-%20FINAL%2001-02-18.pdf
Parise M, Cannon S (2012) Wildfire impacts on processes that generate debris flows in burned watersheds. Nat Hazards 61:217–227
Robichaud P, Wagenbrenner J, Pierson F, Spaeth K, Ashmun L, Moffet C (2016) Infiltration and interrill erosion rates after a wildfire in western Montana, USA. Catena 142:77–88
Roering J, Schmidt K, Stock J, Dietrich W, Montgomery D (2003) Shallow landsliding, root reinforcement, and the spatial distribution of trees in the Oregon coast range. Can Geotech J 40:237–253
Santi P, Morandi L (2013) Comparison of debris-flow volumes from burned and unburned areas. Landslides 10:757–769
Schmidt JC (1995) Geomorphic response to wildfire following timber harvest of a small watershed in southern Oregon. U.S. Geological Survey Water-Resources Investigations Report 94–4122: https://pubs.er.usgs.gov/publication/wri944122
Schmidt KM, Roering JJ, Stock JD, Dietrich WE, Montgomery DR, Schaub T (2001) The variability of root cohesion as an influence on shallow landslide susceptibility in the Oregon Coast Range. Can Geotech J 38(5):995–1024
Slesak R, Schoenholtz S, Evans D (2015) Hillslope erosion two and three years after wildfire, skyline salvage logging, and site preparation in southern Oregon, USA. For Ecol Manag 342:1–7
Spittler T (1995) Fire and the debris flow potential of winter storms. In: Keeley JE, Scott T (eds) Brushfires in California Wildlands: ecology and resource management. International Association of Wildland Fire, Fairfield, pp 113–120
Staley D, Negri J, Kean J, Laber J, Tillery A, Youberg A (2017) Prediction of spatially explicit rainfall intensity–duration thresholds for post-fire debris-flow generation in the western United States. Geomorphology 278:149–162
Swanson FJ (1981) Fire and geomorphic processes, In: Gen. Tech. Rep. USDA Forest Service, WO-26, Washington DC, pp 401–420
U.S. Forest Service (1973) Soil resources inventory. Willamette National Forest, Eugene
U.S. Forest Service (2017) 2017 Pacific Northwest fire narrative: https://www.fs.usda.gov/Internet/FSE_DOCUMENTS/fseprd572804.pdf
U.S. Geological Survey (2017) Milli fire (Deschutes National Forest, OR). Landslides Hazards Program: https://landslides.usgs.gov/hazards/postfire_debrisflow/detail.php?objectid=118
USDA (1999) ROSETTA model. U.S. Salinity Laboratory, Riverside, CA: https://www.ars.usda.gov/pacific-west-area/riverside-ca/us-salinity-laboratory/docs/rosetta-model/
van Genuchten MT (1980) A closed-form equation for predicting the hydraulic conductivity of unsaturated soils. Soil Sci Soc Am J 44:892–898
Vandervaere JP, Vauclin M, Elrick DE (2000) Transient flow from tension infiltrometers II. Four methods to determine sorptivity and conductivity. Soil Sci Soc Am J 64(4):1272–1284
Vieira D, Fernández C, Vega J, Keizer J (2015) Does soil burn severity affect the post-fire runoff and interrill erosion response? A review based on meta-analysis of field rainfall simulation data. J Hydrol 523:452–464
Wells W (1987) The effects of fire on the generation of debris flows in southern California, In: J. E. Costa and G. F. Wieczorek (eds.), Debris Flows/Avalanches: Process, Recognition, and Mitigation. Geological Society of America Review in Engineering Geology 2:105–114
Wells C, Campbell R, DeBano L, Lewis C, Fredriksen R, Franklin E, Froelich R, Dunn P (1979) Effects of fire on soil: a state-of- knowledge review. USDA For Serv Gen Tech Rep WO-7
Westerling A, Hidalgo H, Cayan D, Swetnam T (2006) Warming and earlier spring increase Western U.S. forest wildfire activity. Science 313:936–940
Williams H (1944) Volcanoes of the three sisters region, Oregon cascades. University of California Publications 27:37–84
Wimberly M, Liu Z (2014) Interactions of climate, fire, and management in future forests of the Pacific northwest. For Ecol Manag 327:270–279
Wondzell S, King J (2003) Postfire erosional processes in the Pacific northwest and Rocky Mountain regions. For Ecol Manag 178:75–87
Woods S, Balfour V (2008) The effect of ash on runoff and erosion after a severe forest wildfire, Montana, USA. Int J Wildland Fire 17:535
Woodsmith R, Vache K, McDonnell J, Helvey D (2004) Entiat experimental forest: catchment-scale runoff data before and after a 1970 wildfire. Water Resour J 40:1–5
Woodsmith R, Vache K, McDonnell J, Seibert J, Helvey J (2007) The Entiat experimental forest: a unique opportunity to examine hydrologic response to wildfire. General Technical Report Pacific Northwest Research Station, USDA Forest Service 689:205–216
Zhang R (1997) Determination of soil sorptivity and hydraulic conductivity from the disk infiltrometer. Soil Sci Soc Am J 61(4):1024–1030
Ziemer R, Swanston D (1977) Root strength changes after logging in Southeast Alaska. USDA for. Ser. Pacific northwest Forest and range Experiment Station, Portland, OR., PNW-306:10

Electronic supplementary material The online version of this article (https://doi.org/10.1007/s10346-020-01376-9) contains supplementary material, which is available to authorized users.

S. A. Wall (✉)
Carleton College,
Northfield, MN 55057, USA
Email: sara.wall019@gmail.com

J. J. Roering
Department of Earth Sciences,
University of Oregon,
Eugene, OR 97403-1272, USA

F. K. Rengers
Landslide Hazards Program, Geologic Hazards Science Center,
U.S. Geological Survey,
Golden, CO 80401, USA